AIMS Mathematics, 11(1): 2313–2340.
DOI: 10.3934/math.2026093
Received: 26 November 2025
Revised: 07 January 2026
Accepted: 14 January 2026
Published: 26 January 2026

https://www.aimspress.com/journal/Math

Research article

The exponentiated modified Lindley distribution with diverse biomedical and epidemiological applications

Ammar M. Sarhan[1,2], **Asamh Saleh M. Al Luhayb**[3,*], **Reid Alotaibi**[4] **and M. E. Sobh**[1]

[1] Mathematics Department, Faculty of Science, Mansoura University, Egypt

[2] Department of Mathematics and Statistics, Dalhousie University, Halifax, Nova Scotia, Canada

[3] Department of Mathematics, College of Science, Qassim University, P.O. Box 6644, Buraydah 51452, Saudi Arabia

[4] Department of Mathematics, College of Science and Humanities, Shaqra University, Shaqra, Saudi Arabia

* **Correspondence:** Email: a.alluhayb@qu.edu.sa.

Abstract: This study presents a new two-parameter lifetime model, the exponentiated modified Lindley distribution, which extends the flexibility of the traditional modified Lindley distribution. The proposed model was constructed using an exponentiation approach that introduces an additional shape parameter, allowing it to accommodate a wide variety of data patterns and hazard rate behaviors. Comprehensive analytical properties were investigated, including moments and reliability characteristics, along with several parameter estimation methods. In addition to classical estimation techniques, a Bayesian estimation procedure was developed for the exponentiated modified Lindley distribution, as well as a bootstrap approach for constructing confidence intervals for the model parameters. A simulation study was conducted to assess the efficiency and robustness of the proposed estimators. Furthermore, applications to real datasets demonstrated that the proposed model provides an improved fit compared to conventional lifetime distributions. These results indicate that the exponentiated modified Lindley distribution is a valuable addition to the class of continuous distributions, offering enhanced adaptability for modeling reliability, survival, and other forms of asymmetric data encountered in applied statistics.

Keywords: lifetime modeling; parameter estimation; computational simulations; bootstrap confidence intervals; maximum likelihood estimation; Bayesian inference
Mathematics Subject Classification: 62E10, 62N05, 62F10, 62F15

1. Introduction

Chesneau et al. [4] introduced a generalized form of the Lindley distribution, known as the modified Lindley (ML) distribution. This model is characterized by a single parameter and possesses several desirable statistical properties, offering a middle ground between the exponential and Lindley distributions. Its primary advantage is the enhanced flexibility it provides for modeling lifetime data, making it particularly useful in reliability and survival analysis. The cumulative distribution function (CDF) of the ML distribution is expressed as

$$F_X(x;\theta) = 1 - \left[1 + \frac{\theta x}{1+\theta}\, e^{-\theta x}\right] e^{-\theta x},\ x > 0,\ \theta > 0. \tag{1.1}$$

The corresponding probability density function (PDF) and hazard rate function (HRF) are given, respectively, by

$$f_X(x;\theta) = \frac{\theta}{1+\theta}\, e^{-2\theta x}\left[(1+\theta)e^{\theta x} + 2\theta x - 1\right],\ x > 0,\ \theta > 0\,, \tag{1.2}$$

and

$$h_X(x;\theta) = \frac{\theta(\theta x - 1)}{(1+\theta)e^{\theta x} + \theta x} + \theta,\ x > 0,\ \theta > 0. \tag{1.3}$$

Despite the usefulness of the ML distribution, its single-parameter form restricts its capacity to represent datasets with varying levels of skewness and dispersion. Adding an extra parameter can significantly enhance its flexibility, enabling it to capture diverse distributional shapes observed in complex real-world applications. To overcome the limitations of the original ML distribution, several generalized versions have been introduced in the literature. Examples include the Marshall–Olkin modified Lindley (MOML) distribution [8], the sine modified Lindley (SML) distribution [19], the power modified Lindley (PML) distribution [13], and the new Lindley extension (NLE) distribution [11], each proposing distinctive structural adjustments that yield improved modeling performance.

In this paper, we extend the ML distribution by applying the exponentiation technique introduced by Zacks [20] and then applied by several authors, among them are Mudholkar and Srivastava [14], Gupta and Kundu [10], Sarhan and Kundu [17], Sarhan and Apaloo [15], and Sarhan et al. [16]. The resulting model, termed the exponentiated modified Lindley (EML) distribution, incorporates an additional shape parameter that increases its flexibility and enhances its capability to represent a wider variety of data patterns.

The EML distribution is particularly useful in survival analysis, where it can characterize different forms of lifetime behavior associated with biological organisms, medical treatment outcomes, and the durability of mechanical devices. In reliability engineering, it provides an effective framework for modeling the operational lifespan of industrial components and systems under varying stress conditions. Beyond these areas, the EML distribution also proves valuable in environmental studies for modeling extreme phenomena, in actuarial science for assessing insurance-related risks, and in financial applications where skewed or heavy-tailed loss data often arise. Its ability to accommodate diverse distributional shapes makes it a versatile and powerful tool for analyzing a wide range of real-world datasets.

The remainder of this paper is structured as follows. Section 2 introduces the formulation of the proposed model and discusses the asymptotic behavior of both the PDF and HRF, and the effects

of the shape parameters. Section 3 explores several important statistical properties of the EML distribution, including its quantile, moments, moment generating function, incomplete moments, skewness, and kurtosis. Moreover, Section 4 develops the estimation framework for the EML distribution, encompassing classical approaches, a tailored Bayesian estimation algorithm, and a bootstrap procedure for constructing confidence intervals. Section 5 presents a simulation setup and a comparative analysis of maximum likelihood estimation and Bayesian estimators, evaluating their accuracy and reliability using average point estimates (APEs), mean square errors (MSEs), and coverage probabilities (CPs) of 95% confidence and credible intervals across different sample sizes. Section 6 showcases the versatility of the EML model and its robust estimation framework through applications to four medical datasets. Finally, Section 7 summarizes the key findings, highlights the advantages of the EML distribution, and outlines potential avenues for future research.

2. The exponentiated modified Lindley distribution

The CDF of the EML distribution is obtained by raising the CDF of the ML distribution to a power α, where $\alpha > 0$. That is, the CDF of the EML distribution is defined as

$$F(x;\theta,\alpha) = [F_X(x;\theta)]^{\alpha} = \left[1 - \left(1 + \frac{\theta x}{1+\theta}\, e^{-\theta x}\right) e^{-\theta x}\right]^{\alpha}, \; x > 0, \; \theta, \alpha > 0. \tag{2.1}$$

The PDF of the EML distribution is given as

$$f(x;\theta,\alpha) = \frac{\alpha\theta\left[(1+\theta)e^{\theta x} + 2\theta x - 1\right] e^{-2\theta x}}{1+\theta} \left[1 - \left(1 + \frac{\theta x}{1+\theta}\, e^{-\theta x}\right) e^{-\theta x}\right]^{\alpha-1}. \tag{2.2}$$

The corresponding survival function is obtained as

$$S(x;\theta,\alpha) = 1 - \left[1 - \left(1 + \frac{\theta x}{1+\theta}\, e^{-\theta x}\right) e^{-\theta x}\right]^{\alpha}. \tag{2.3}$$

Using the results presented in Eqs (2.1) and (2.2), the corresponding HRF can be expressed as

$$h(x;\theta,\alpha) = \frac{\alpha\theta e^{-2\theta x}\left[(1+\theta)e^{\theta x} + 2\theta x - 1\right]\left[1 - \left(1 + \frac{\theta x}{1+\theta}\, e^{-\theta x}\right) e^{-\theta x}\right]^{\alpha-1}}{(1+\theta)\left\{1 - \left[1 - \left(1 + \frac{\theta x}{1+\theta}\, e^{-\theta x}\right) e^{-\theta x}\right]^{\alpha}\right\}} \tag{2.4}$$

and the reversed hazard rate function is given in the form

$$r(x;\theta,\alpha) = \frac{\alpha\theta e^{-2\theta x}\left[(1+\theta)e^{\theta x} + 2\theta x - 1\right]}{(1+\theta)\left[1 - \left(1 + \frac{\theta x}{1+\theta}\, e^{-\theta x}\right) e^{-\theta x}\right]}. \tag{2.5}$$

We note that the parameter α serves as a shape parameter, controlling the accumulation of probability mass. It affects the shape and concentration of the PDF without altering the scale parameter θ. The following two subsections examine the limiting behavior of the model and illustrate the effect of α on both the PDF and the HRF of the EML distribution.

2.1. Asymptotic behavior of the PDF

For small values of x (i.e., as $x \to 0$), we have

$$\frac{\alpha\theta[(1+\theta)e^{\theta x} + 2\theta x - 1]\, e^{-2\theta x}}{1+\theta} \sim \frac{\alpha\theta^2}{1+\theta}.$$

Moreover, using the expansions $e^{-\theta x} = 1 - \theta x + O(x^2)$ and $e^{-2\theta x} = 1 - 2\theta x + O(x^2)$, it follows that

$$\left[1 - \left(1 + \frac{\theta x}{1+\theta}\, e^{-\theta x}\right) e^{-\theta x}\right]^{\alpha-1} = \left[\frac{\theta^2 x}{1+\theta} + O(x^2)\right]^{\alpha-1} \sim \left(\frac{\theta^2 x}{1+\theta}\right)^{\alpha-1},$$

where $O(x^2)$ represents terms that vanish at least as fast as x^2 near zero. Consequently,

$$f(x;\theta,\alpha) \sim \frac{\alpha\theta^2}{1+\theta}\left(\frac{\theta^2 x}{1+\theta}\right)^{\alpha-1} = \frac{\alpha\theta^{2\alpha}}{(1+\theta)^{\alpha}}\, x^{\alpha-1}, \qquad (x \to 0).$$

Therefore, the asymptotic behavior of the PDF as $x \to 0$ is given by

$$\lim_{x\to 0} f(x;\theta,\alpha) = \begin{cases} 0, & \alpha > 1, \\ \dfrac{\theta^2}{1+\theta}, & \alpha = 1, \\ \infty, & 0 < \alpha < 1. \end{cases} \qquad (2.6)$$

Moreover, the limit behavior of the PDF of the EML distribution as $x \to \infty$ is given as

$$\lim_{x\to\infty} f(x;\theta,\alpha) = 0.$$

Furthermore, since the PDF of the EML can be expressed in the form

$$f(x;\theta,\alpha) = \alpha f_X(x;\theta)\,[F_X(x;\theta)]^{\alpha-1},$$

the factor $[F_X(x;\theta)]^{\alpha-1}$ directly governs the shape of the density as:

- For $\alpha > 1$, this term suppresses the density near the origin, causing the PDF to flatten near $x = 0$ and shift its mode toward larger x. The distribution therefore becomes more spread out and assigns greater probability to larger values.
- For $\alpha < 1$, the opposite occurs: The density is amplified near $x = 0$, producing a sharply peaked PDF that concentrates probability close to the origin.

In summary, increasing α shifts the distribution to the right and increases its spread, while decreasing α shifts it to the left and increases the concentration near smaller values of x. Thus, α determines how rapidly the distribution accumulates probability and where the bulk of its mass lies.

2.2. *Asymptotic behavior of the HRF*

Based on the results in Eq (2.6), the HRF exhibits the same limiting behavior as the PDF. Furthermore, since the HRF can be defined as

$$h(x;\theta,\alpha) = \frac{f(x;\theta,\alpha)}{1-F(x;\theta,\alpha)} = \frac{\alpha f_X(x;\theta)\,[F_X(x;\theta)]^{\alpha-1}}{1-[F_X(x;\theta)]^{\alpha}},$$

we note that the direction of the hazard rate depends on the value of α. In other words, increasing α lowers the instantaneous failure rate (or hazard) at every x. This reduction becomes negligible in the right tail as the survival probability approaches zero. Hence, larger α values correspond to a more resilient system or process, where failure becomes less likely at each fixed time x.

We present the possible shapes of the PDF and HRF of the EML distribution for different values of α and θ in Figures 1 and 2, respectively.

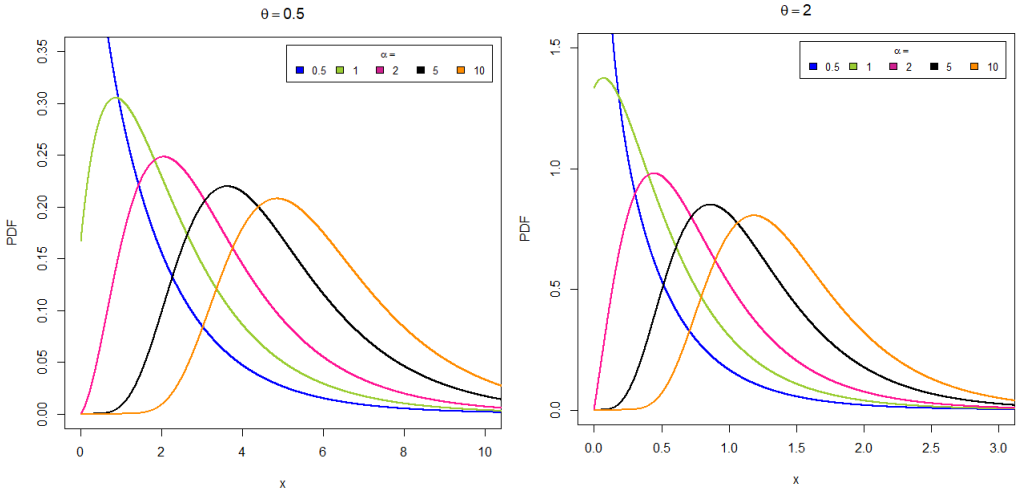

Figure 1. The PDF of the EML models at different values of α and θ.

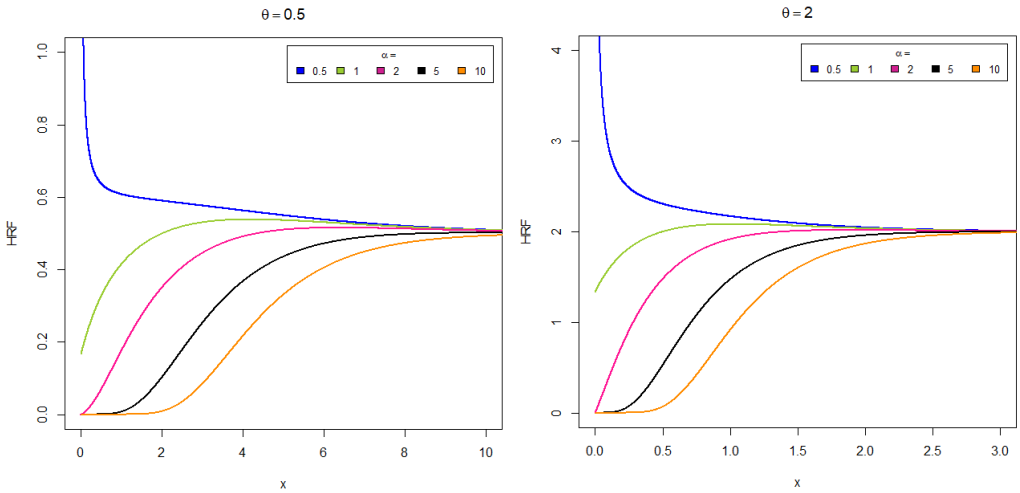

Figure 2. The HRF of the EML models at different values of α and θ.

3. Statistical properties

Let X follow EML(θ, α), and then we can get the qth quantile by solving the following equation in x:

$$g(x) = 1 - q^{\frac{1}{\alpha}} - \left[1 + \frac{\theta x}{1+\theta} e^{-\theta x}\right] e^{-\theta x} = 0\,,\ q \in (0,1). \tag{3.1}$$

Equation (3.1) lacks a closed-form analytic solution for x. To determine the quantile for EML(θ, α), we must solve this equation numerically. A suitable approach is the bisection method, a reliable numerical technique that finds roots of a continuous function on a specified interval. This method iteratively narrows the interval containing the root, ensuring convergence to the desired solution.

Figure 3 illustrates the quantile function defined in Eq (3.1) for representative values of α and θ. The figure demonstrates how the distribution of the variable characterized by its quantiles (Q_1, median, and Q_3) changes under different parameter settings. The main observations drawn from Figure 3 are summarized below:

- **Quantiles as a function of α (with θ fixed):** Smaller values of α correspond to distributions with greater skewness and dispersion, whereas larger α values produce less skewed and more concentrated distributions.
- **Quantiles as a function of θ (with α fixed):** The parameter θ primarily influences the horizontal position of the quantiles without substantially altering the overall shape, skewness, or relative spread (e.g., the interquartile range-to-median ratio). Its effect is largely one of stretching rather than reshaping.

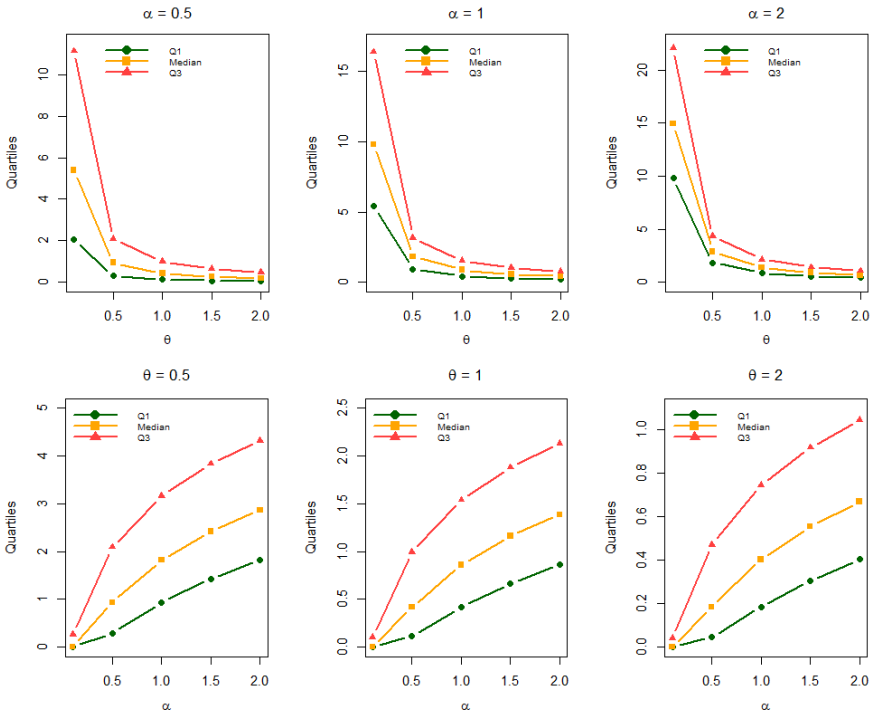

Figure 3. Fundamental quantiles (Q_1, median, Q_3) obtained for several values of the parameters θ and α.

3.1. Various measures of moments

The $r-$th ordinary moment of the EML distribution can be written as

$$\mu_r^{'} = \int_0^{\infty} x^r f(x;\theta,\alpha)dx = \sum_{i=0}^{\infty}\sum_{j=0}^{i}\psi_{r,i,j}(\alpha,\theta)\left(\frac{\theta+1}{(i+j+1)^{r+j+1}} + \frac{2(r+j)+1}{(i+j+2)^{r+j+1}}\right), \tag{3.2}$$

where $\psi_{r,i,j}(\alpha,\theta) = \binom{\alpha-1}{i}\binom{i}{j}\frac{(-1)^j\alpha\Gamma(r+j+1)}{\theta^r(1+\theta)^{j+1}}$.

The moment-generating function is expressed as

$$\begin{aligned} M_X(t) &= \int_0^t e^{tx} f(x;\theta,\alpha)dx \\ &= \sum_{s=0}^{\infty}\sum_{i=0}^{\infty}\sum_{j=0}^{i}\frac{t^s\psi_{s,i,j}(\alpha,\theta)}{s!}\left(\frac{\theta+1}{(i+j+1)^{s+j+1}} + \frac{2(s+j)+1}{(i+j+2)^{s+j+1}}\right). \end{aligned} \tag{3.3}$$

The $r-$th incomplete moment of the EML distribution is determined by

$$\begin{aligned} I_r(t) &= \int_0^t x^r f(x;\theta,\alpha)dx \\ &= \sum_{i=0}^{\infty}\sum_{j=0}^{i}\phi_{r,i,j}(\alpha,\theta)\left(\frac{(\theta+1)\,\kappa_{r,i,j}(\theta;t)}{(i+j+1)^{\,r+j+1}} + \frac{\kappa_{r,i,j}(\theta;t) - 2t^{r+j+1}e^{-(i+j+2)\theta t}}{(i+j+2)^{\,r+j+1}}\right), \end{aligned} \tag{3.4}$$

where $\phi_{r,i,j}(t;\alpha,\theta) = \binom{\alpha-1}{i}\binom{i}{j}\frac{(-1)^j\alpha}{\theta^r(1+\theta)^{j+1}}$, $\kappa_{r,i,j}(\theta;t) = \gamma(r+j+1,(i+j+1)\theta t)$, and $\gamma(s,t) = \int_0^t v^{s-1}e^{-v}dv$ is the lower incomplete gamma function.

Using the first four ordinary moments of the EML distribution, the corresponding measures of skewness $\mathcal{S}k(Y)$ and kurtosis $\mathcal{K}u(Y)$ can be derived as follows:

$$\mathcal{S}k(Y) = \frac{\mu_3^{'} - 3\mu_1^{'}\mu_2^{'} + 2(\mu_1^{'})^3}{\left[\mu_2^{'} - (\mu_1^{'})^2\right]^{\frac{3}{2}}} \tag{3.5}$$

and

$$\mathcal{K}u(Y) = \frac{\mu_4^{'} - 4\mu_1^{'}\mu_3^{'} + 6(\mu_1^{'})^2\mu_2^{'} - 3(\mu_1^{'})^4}{\left[\mu_2^{'} - (\mu_1^{'})^2\right]^2}. \tag{3.6}$$

Table 1 presents the descriptive statistics of the EML distribution based on its first four raw moments. The table lists the values of the mean ($\mu_1^{'}$), variance (σ^2), skewness ($\mathcal{S}k(Y)$), and kurtosis ($\mathcal{K}u(Y)$) for various combinations of the parameters α and θ. These statistics describe how the location, spread, and shape of the distribution change as the values of the parameters vary.

From Table 1, it is observed that the mean and higher-order moments decrease as θ increases, indicating that larger values of the scale parameter shift the distribution toward smaller magnitudes. The variance also decreases with higher θ, showing that the distribution becomes more concentrated around the mean. Conversely, increasing the shape parameter α leads to higher mean and variance values, suggesting a wider and more dispersed form. Moreover, it is evident that both skewness and

kurtosis are influenced by the parameters α and θ. As α increases, the distribution tends to become more positively skewed while its kurtosis decreases, indicating a flatter peak. In contrast, increasing θ generally reduces both skewness and kurtosis, suggesting a more symmetric and lighter-tailed form. Overall, these results demonstrate the EML distribution's flexibility in modeling data with different degrees of asymmetry and tail thickness.

Table 1. Descriptive statistics of the EML distribution.

α	θ	$\mu_1^{'}$	$\mu_2^{'}$	$\mu_3^{'}$	$\mu_4^{'}$	σ^2	$\mathcal{S}k(Y)$	$\mathcal{K}u(Y)$
	0.1	2.2508	31.9211	789.8869	27625.36	25.9444	4.2824	28.3789
	0.5	0.4002	1.1398	5.6279	38.8189	0.9862	4.7875	35.8969
0.1	1.0	0.1855	0.2763	0.7046	2.4879	0.2489	5.1235	40.3393
	2.0	0.0859	0.0642	0.0839	0.1537	0.0570	5.2392	42.5185
	5.0	0.0332	0.0099	0.0054	0.0042	0.0092	5.5169	47.5184
	0.1	8.0943	139.7546	3783.905	141533.3	74.5460	3.0711	10.9869
	0.5	1.5026	5.2363	28.7027	219.2054	2.9569	2.9413	11.2849
0.5	1.0	1.5026	1.2335	3.4049	13.0962	0.7323	2.9234	11.3832
	2.0	0.3398	0.2965	0.4144	0.7948	0.1849	2.9517	11.9916
	5.0	0.1285	0.0456	0.0257	0.0197	0.0287	2.9671	12.3605
	0.1	12.2858	247.4630	7103.4010	269200.4	96.1352	3.8399	8.8623
	0.5	2.3328	9.2870	53.0554	399.9258	3.8859	3.4908	8.4828
1	1.0	1.1258	2.2689	6.6329	25.6757	0.9789	3.3262	8.4791
	2.0	0.5448	0.5434	0.8079	1.6182	0.2518	3.2000	8.7910
	5.0	0.2079	0.0829	0.0484	0.0373	0.0396	3.0964	8.8650
	0.1	17.2107	409.4108	12715.89	497387.3	110.7000	5.9768	7.4931
	0.5	3.3442	15.7249	98.6770	790.1646	4.6498	5.3037	7.2397
2	1.0	1.6284	3.8553	12.2584	50.1418	1.1795	4.9809	7.3914
	2.0	0.9589	0.9293	1.4703	2.9785	0.2990	4.6292	7.0342
	5.0	0.3106	0.1437	0.0917	0.0752	0.0497	4.3145	7.2078
	0.1	20.4302	535.8324	17776.13	731166.9	119.6287	8.0014	6.7077
	0.5	3.9929	20.8924	139.6440	1165.54	4.9810	7.2015	6.7201
3	1.0	1.9621	5.0955	17.0857	71.7469	1.2856	6.6839	6.9445
	2.0	0.9589	1.2507	2.1031	4.4162	0.3276	6.1774	6.5461
	5.0	0.3773	0.1934	0.1296	0.1086	0.0538	5.7768	6.5669
	0.1	22.7655	643.3591	22370.18	947561.2	125.5584	9.8296	6.4735
	0.5	4.4726	25.04817	174.4835	1487.038	5.1248	9.1116	6.2679
4	1.0	2.1992	6.1763	21.5939	92.1937	1.3156	8.4429	6.1764
	2.0	1.0807	1.5117	2.6603	5.7733	0.3349	7.8928	6.1296
	5.0	0.4260	0.2353	0.1641	0.1404	0.0556	7.3195	6.5436
	0.1	27.5197	894.5016	34265.56	1549907	134.4116	14.7398	6.1442
	0.5	5.4324	34.9573	266.2326	2387.277	5.5144	13.7353	6.1926
7	1.0	2.6917	8.6207	32.8857	148.2505	1.4094	12.9795	6.0167
	2.0	1.3285	2.1390	4.1171	9.4242	0.3599	12.1729	6.0272
	5.0	0.5259	0.3344	0.2556	0.2320	0.0587	11.5084	5.7421

4. Parameters' estimation

In this section, we investigate parameter estimation by applying multiple estimation methods, comparing their assumptions, strengths, and suitability for the data at hand.

4.1. The maximum likelihood method

The likelihood function, for a simple random sample $x_1, x_2, \cdots, x_n$ taken from the EML(θ, α), is given in the form

$$L(\theta,\alpha) = \frac{\alpha^n\theta^n}{(\theta+1)^n}\prod_{i=1}^{n}\left[(1+\theta)e^{\theta x_i}+2\theta x_i-1\right]e^{-2\theta x_i}\left[1-\left(1+\frac{\theta x_i}{1+\theta}e^{-\theta x_i}\right)e^{-\theta x_i}\right]^{\alpha-1}. \tag{4.1}$$

The log-likelihood function is

$$\begin{aligned}\mathcal{L}(\theta,\alpha) &= n\ln\alpha + n\ln\theta - n\ln(1+\theta) - 2\theta\sum_{i=1}^{n}x_i + \sum_{i=1}^{n}\ln\left[(1+\theta)e^{\theta x_i}+2\theta x_i-1\right]\\ &\quad + (\alpha-1)\sum_{i=1}^{n}\ln\left[1-\left(1+\frac{\theta x_i}{1+\theta}e^{-\theta x_i}\right)e^{-\theta x_i}\right].\end{aligned}$$

$$\begin{aligned}\frac{\partial\mathcal{L}}{\partial\theta} &= \frac{n}{\theta}-\frac{n}{1+\theta}-2\sum_{i=1}^{n}x_i+\sum_{i=1}^{n}\frac{(1+\theta)x_ie^{\theta x_i}+e^{\theta x_i}+2x_i}{(1+\theta)e^{\theta x_i}+2\theta x_i-1}\\ &\quad +(\alpha-1)\sum_{i=1}^{n}\frac{x_ie^{\theta x_i}(1+\theta)^2+2\theta(1+\theta)x_i^2-x_i}{(1+\theta)^2e^{2\theta x_i}\left[1-\left(1+\frac{\theta x_i}{1+\theta}\right)e^{-\theta x_i}\right]};\end{aligned} \tag{4.2}$$

$$\frac{\partial\mathcal{L}}{\partial\alpha} = \frac{n}{\alpha}+\sum_{i=1}^{n}\ln\left[1-\left(1+\frac{\theta x_i}{1+\theta}e^{-\theta x_i}\right)e^{-\theta x_i}\right]. \tag{4.3}$$

Using Eq (4.3), we obtain

$$\hat{\alpha} = -\frac{n}{\sum_{i=1}^{n}\ln\left[1-\left(1+\frac{\theta x_i}{1+\theta}e^{-\theta x_i}\right)e^{-\theta x_i}\right]}. \tag{4.4}$$

By substituting expression (4.4) into the right-hand side of Eq (4.2), the maximum likelihood estimate (MLE) of θ is obtained numerically by solving the following equation:

$$\begin{aligned}&\frac{n}{\theta}-\frac{n}{1+\theta}-2\sum_{i=1}^{n}x_i+\sum_{i=1}^{n}\frac{(1+\theta)x_ie^{\theta x_i}+e^{\theta x_i}+2x_i}{(1+\theta)e^{\theta x_i}+2\theta x_i-1}\\ &+\left(-\frac{n}{\sum_{i=1}^{n}\ln\left[1-\left(1+\frac{\theta x_i}{1+\theta}e^{-\theta x_i}\right)e^{-\theta x_i}\right]}-1\right)\sum_{i=1}^{n}\frac{x_ie^{\theta x_i}(1+\theta)^2+2\theta(1+\theta)x_i^2-x_i}{(1+\theta)^2e^{2\theta x_i}\left[1-\left(1+\frac{\theta x_i}{1+\theta}\right)e^{-\theta x_i}\right]}=0.\end{aligned} \tag{4.5}$$

Equation (4.5) does not have a closed-form analytical solution for θ; therefore, a numerical approach is required. In this study, the bisection method is employed to obtain a numerical estimate of θ, and the algorithm is implemented using the R software environment.

To construct confidence intervals for the vector of parameters $\eta = (\theta, \alpha)$, we utilize the asymptotic properties of the MLEs. Under the standard regularity assumptions, the MLE vector $\hat{\eta} = (\hat{\theta}, \hat{\alpha})$ follows an approximate normal distribution $\mathbf{N}(\eta, \triangle_n^{-1}(\eta))$, where $\triangle_n(\eta)$ is the expected Fisher information matrix given by:

$$\triangle_n(\eta) = -\mathbb{E}\left[\frac{\partial^2 \mathcal{L}}{\partial \eta\, \partial \eta^T}\right] = -\mathbb{E}\begin{pmatrix} \frac{\partial^2 \mathcal{L}}{\partial \theta^2} & \frac{\partial^2 \mathcal{L}}{\partial \theta \partial \alpha} \\ \frac{\partial^2 \mathcal{L}}{\partial \alpha \partial \theta} & \frac{\partial^2 \mathcal{L}}{\partial \alpha^2} \end{pmatrix}. \tag{4.6}$$

Since the analytical expressions for the expected second-order partial derivatives of $\mathcal{L}$ are intractable, the Fisher information matrix cannot be obtained in closed form. Therefore, we employ the observed Fisher information matrix as a practical alternative. This matrix is evaluated by substituting the unknown parameters θ and α with their corresponding MLEs, $\hat{\theta}$ and $\hat{\alpha}$, respectively. The resulting observed information provides a consistent estimate of the true Fisher information and can be used for large-sample inference, including the estimation of standard errors and the construction of confidence intervals. The observed Fisher information matrix is given as

$$\mathcal{F}(\hat{\eta}) = -\left.\begin{pmatrix} \frac{\partial^2 \mathcal{L}}{\partial \theta^2} & \frac{\partial^2 \mathcal{L}}{\partial \theta \partial \alpha} \\ \frac{\partial^2 \mathcal{L}}{\partial \alpha \partial \theta} & \frac{\partial^2 \mathcal{L}}{\partial \alpha^2} \end{pmatrix}\right|_{\theta=\hat{\theta},\, \alpha=\hat{\alpha}}. \tag{4.7}$$

By inverting the information matrix, one can obtain the asymptotic variances and covariances of the MLEs corresponding to the vector $\hat{\eta}$. Moreover, the approximate $100(1-\delta)\%$ confidence intervals (CI) for the vector of parameters η can then be constructed as follows:

$$\hat{\eta}_i \pm z_{1-\frac{\delta}{2}} \sqrt{\mathbb{V}(\hat{\eta}_i)},\ i = 1, 2,$$

where $\mathbb{V}(\hat{\eta}_i)$ is the ith diagonal element of the inverse observed Fisher information matrix $\mathcal{F}^{-1}(\hat{\eta})$ and z_q is the upper qth quantile of the standard normal distribution.

4.2. Likelihood intervals

In many parametric settings, closed-form expressions for the sampling distributions of MLEs are not available. In such cases, likelihood-based interval estimation offers a practical and theoretically grounded alternative. For each model parameter, we construct what we refer to as a maximum likelihood interval (MLI), derived from the corresponding relative profile likelihood function.

Let $\mathcal{L}(\theta, \alpha)$ denote the log-likelihood function, and let $(\hat{\theta}, \hat{\alpha})$ be the MLEs obtained from the sample. For a fixed parameter of interest θ, the profile log-likelihood is defined as

$$\mathcal{L}_{\mathrm{p}}(\theta) = \mathcal{L}(\theta,\, \hat{\alpha}),$$

that is, by fixing θ and maximizing the log-likelihood with respect to the nuisance parameter α. The $100p\%$ MLI for θ is the set of values satisfying $r(\theta) \geq \log p,\ 0 < p < 1$ (see [12]), where $r(\theta)$ is the relative log-likelihood for θ defined by $r(\theta) = \mathcal{L}_{\mathrm{p}}(\theta) - \mathcal{L}(\hat{\theta}, \hat{\alpha})$.

An analogous procedure yields the MLI for the second parameter α. The $100p\%$ MLI for α is the set of α values satisfying the inequality $r(\alpha) = \mathcal{L}(\hat{\theta},\, \alpha) - \mathcal{L}(\hat{\theta}, \hat{\alpha}) \geq \log p$.

For clarity, we note that, asymptotically, a $100(1-\delta)\%$ confidence interval (CI) coincides with a $100p\%$ MLI, where

$$p = \exp\Big\{-\tfrac{1}{2}\chi^2_{1,\,1-\delta}\Big\}.$$

For example, a 95% CI corresponds to a 14.7% MLI. To illustrate the connection between the standard likelihood ratio χ^2 approximation and the MLI, we provide further details in Appendix A.

Because the profile likelihood functions for θ and α do not yield closed-form solutions for these inequalities, numerical optimization is required. In this study, the MLIs are computed using iterative root-finding techniques, such as the Newton–Raphson algorithm. The resulting likelihood intervals are presented in the application section, where they provide a likelihood-based quantification of uncertainty for the parameter estimates.

4.3. Bootstrap confidence intervals

Bootstrap methods, introduced by Efron [6], offer a flexible nonparametric framework for approximating the sampling distribution of a statistic and for constructing confidence intervals when analytic derivations are unavailable or intractable (see Davison and Hinkley [5]). Let $\hat{\theta} = s(X)$ denote an estimator of a parameter of interest θ, such as a mean, variance, or regression coefficient, computed from an observed random sample $X = (x_1, x_2, \ldots, x_n)$. The bootstrap procedure involves repeatedly resampling, with replacement, from the original data to generate B bootstrap samples, denoted as $X^{*(1)}, X^{*(2)}, \ldots, X^{*(B)}$. For each bootstrap sample, we compute the corresponding statistic $\hat{\theta}^{*(b)} = s(X^{*(b)})$. The empirical distribution of $\{\hat{\theta}^{*(1)}, \hat{\theta}^{*(2)}, \ldots, \hat{\theta}^{*(B)}\}$ serves as an estimate of the sampling distribution of $\hat{\theta}$.

Several types of bootstrap confidence intervals (CIs) can be constructed from these resamples. Appendix B describes four commonly used approaches to bootstrap confidence intervals.

The following algorithm outlines the computational steps that can be implemented in R to obtain the four types of bootstrap confidence intervals described in Appendix B.

Algorithm 1: Bootstrap confidence intervals for a parameter θ.

Input: Sample $x = (x_1, \ldots, x_n)$, number of bootstrap samples B
Output: Normal, Basic, Percentile, and BCa confidence intervals for θ
for $b = 1$ **to** B **do**
  Draw a bootstrap sample $x^{*(b)}$ of size n from x;
  Compute $\hat{\theta}^{*(b)} = s(x^{*(b)})$;
Compute $\widehat{SE}_{boot} = \sqrt{\frac{1}{B-1}\sum_{b=1}^{B}(\hat{\theta}^{*(b)} - \bar{\hat{\theta}}^{*})^2}$;
Normal CI: $\hat{\theta} \pm z_{\delta/2}\,\widehat{SE}_{boot}$;
Basic CI: $(2\hat{\theta} - \hat{\theta}^{*}_{(1-\delta/2)},\ 2\hat{\theta} - \hat{\theta}^{*}_{(\delta/2)})$;
Percentile CI: $(\hat{\theta}^{*}_{(\delta/2)},\ \hat{\theta}^{*}_{(1-\delta/2)})$;
BCa CI: $\left(\hat{\theta}^{*}_{\Phi(z_0+\frac{z_0+z_{\delta/2}}{1-a(z_0+z_{\alpha/2})})},\ \hat{\theta}^{*}_{\Phi(z_0+\frac{z_0+z_{1-\delta/2}}{1-a(z_0+z_{1-\alpha/2})})}\right)$.

As shown in Algorithm 1, the lower bounds of the normal and basic bootstrap confidence intervals may become negative when $\hat{\theta} < z_{\delta/2}\widehat{SE}\text{boot}$ and $\hat{\theta} < \frac{1}{2}\hat{\theta}^{*}(1-\delta/2)$, respectively. Since the model parameters are restricted to be non-negative, these two types of confidence intervals are therefore not recommended in this setting.

4.4. Bayesian method

In this section, we employ the Bayesian approach to estimate the two parameters of the EML(θ, α) distribution. Since both parameters are positive, we assume that they are independent and follow gamma prior distributions with hyperparameters (a_1, b_1) and (a_2, b_2) corresponding to θ and α, respectively. The joint prior density of (θ, α), up to a normalized constant, is

$$g(\theta, \alpha) \propto \theta^{a_1-1}\alpha^{a_2-1}e^{-b_1\theta-b_2\alpha}. \tag{4.8}$$

Combining the prior density in (4.8) with the likelihood function in (4.1), we can derive the posterior density function of (θ, α), given data x, up to a normalized constant, using Bayes' theorem.

$$g(\theta, \alpha \mid x) \propto \frac{\alpha^{n+a_2-1}\,\theta^{n+a_1-1}}{(1+\theta)^n}\, e^{-b_1\theta-b_2\alpha} \prod_{i=1}^{n}\Big[(1+\theta)e^{\theta x_i} + 2\theta x_i - 1\Big]e^{-2\theta x_i}$$
$$\times\left[1-\left(1+\frac{\theta x_i}{1+\theta}e^{-\theta x_i}\right)e^{-\theta x_i}\right]^{\alpha-1}.$$

It is clear that the posterior distribution of (θ, α) does not belong to any standard family of distributions, and the corresponding normalizing constant cannot be evaluated analytically. To overcome this challenge, we employ the Markov chain Monte Carlo (MCMC) method to generate samples directly from the posterior distribution without requiring the computation of the normalizing constant. The simulated draws are then used to approximate the Bayesian point estimates, credible intervals, and other posterior summaries.

To implement the MCMC algorithm, an appropriate proposal distribution that approximates the shape of the posterior distribution and is easy to sample from must be selected. A natural choice is the bivariate normal distribution; however, since the normal distribution is defined over the entire real line, it does not align with the support of the model parameters, which are strictly positive. To address this issue, we apply a logarithmic transformation to the parameters such that $\phi_1 = \log(\theta) \in \mathbb{R}$ and $\phi_2 = \log(\alpha) \in \mathbb{R}$. This transformation allows us to use a bivariate normal proposal distribution to generate samples for the transformed parameters (ϕ_1, ϕ_2). Once the MCMC sampling is completed, the inverse transformation is applied to obtain the corresponding chain of simulated samples for the original parameters (θ, α).

Explanation. This algorithm (Algorithm 2) implements a random walk Metropolis–Hastings (RWMH) sampler to obtain draws from the posterior distribution of the transformed parameters $(\phi_1, \phi_2) = (\log\theta, \log\alpha)$ given the observed data x. A bivariate normal proposal distribution is used with mean equal to the current state and covariance matrix Σ. Each proposed point is accepted or rejected based on the Metropolis–Hastings acceptance probability r. After generating N posterior draws, the inverse transformations $\theta = e^{\phi_1}$ and $\alpha = e^{\phi_2}$ are applied to recover samples on the original scale of the model parameters. These posterior samples are then used to compute Bayesian estimates, credible intervals, and diagnostic plots.

Algorithm 2: Random walk Metropolis–Hastings for $g(\phi_1, \phi_2 \mid y)$.

Input: Data y, initial $(\phi_1^{(0)}, \phi_2^{(0)})$, iterations N, covariance Σ
Output: Posterior samples $\{(\theta^{(t)}, \alpha^{(t)})\}_{t=1}^{N}$
for $t = 1$ **to** N **do**
  Generate proposal: $(\phi_1^*, \phi_2^*) \sim \mathcal{N}_2((\phi_1^{(t-1)}, \phi_2^{(t-1)}), \Sigma)$;
  Compute acceptance ratio: $r = \dfrac{g(\phi_1^*, \phi_2^* \mid y)}{g(\phi_1^{(t-1)}, \phi_2^{(t-1)} \mid y)}$;
  Draw $u \sim \text{Uniform}(0, 1)$;
  if $u < \min(1, r)$ **then**
    $(\phi_1^{(t)}, \phi_2^{(t)}) \leftarrow (\phi_1^*, \phi_2^*)$;
  else
    $(\phi_1^{(t)}, \phi_2^{(t)}) \leftarrow (\phi_1^{(t-1)}, \phi_2^{(t-1)})$;
Compute transformed parameters: $\theta^{(t)} = e^{\phi_1^{(t)}}$, $\alpha^{(t)} = e^{\phi_2^{(t)}}$ for $t = 1, \ldots, N$;
return $\{(\theta^{(t)}, \alpha^{(t)})\}_{t=1}^{N}$.

5. Simulation study

In this section, we present a simulation study designed to evaluate and compare the performance of ML and Bayesian estimation methods for the parameters (θ, α) of the EML distribution. The primary goal of this study is to assess the accuracy and reliability of both estimation approaches in terms of the APEs, MSEs, and CPs of 95% confidence and credible intervals under different sample sizes and parameter settings.

5.1. Simulation design

Independent random samples of sizes $n = 30, 50, 100, 150, 200$, and 500 were generated from the EML distribution. The random samples were simulated using the inverse transform method derived from the cumulative distribution function of the EML distribution. To examine the effects of different parameter combinations, we considered three parameter settings: $(\theta, \alpha) = (1.5, 2.0)$, $(2.0, 3.0)$, and $(3.0, 5.0)$. These parameter values were chosen to reflect typical behavior of the EML distribution.

For each parameter setting and sample size, $M = 2000$ replications were generated. For every replication, both the ML and Bayesian estimation methods were applied, and the corresponding estimates of θ and α were recorded.

5.2. Estimation procedures

For the maximum likelihood estimation, the log-likelihood function of the EML model was maximized numerically using the `optim()` function in R, employing the BFGS quasi-Newton optimization algorithm. The observed Fisher information matrix was used to approximate the standard errors and construct the asymptotic 95% confidence intervals for θ and α.

For the Bayesian estimation, we assumed independent gamma priors for both parameters, $\theta \sim \text{Gamma}(a_1, b_1)$ and $\alpha \sim \text{Gamma}(a_2, b_2)$, with small hyperparameter values $(a_1, a_2, b_1, b_2) = (0.001, 0.001, 0.001, 0.001)$ to represent vague or noninformative priors. Since the posterior

distribution does not have a closed form, we implemented the Metropolis–Hastings algorithm within a Markov chain Monte Carlo (MCMC) framework to generate posterior samples. The proposal distribution was chosen to be a bivariate normal on the log-transformed parameters $(\phi_1, \phi_2) = (\log\theta, \log\alpha)$, ensuring that the back-transformed values remain positive, and the variance–covariance matrix is obtained as the inverse of the observed Fisher information matrix for the transformed parameters. Each chain consisted of 15000 iterations, with the first 5000 discarded as burn-in. Convergence diagnostics, including trace plots and autocorrelation functions, confirmed satisfactory convergence and mixing of the simulated chains.

5.3. Evaluation criteria

The performance of both estimation methods was evaluated using the following summary statistics, computed across all $M = 2000$ replications:

(1) The APE of each parameter, given by $\bar{\psi} = \dfrac{1}{M}\sum_{i=1}^{M}\hat{\psi}_i$, where $\psi \in \{\theta, \alpha\}$.

(2) The MSE, defined as $\mathrm{MSE}(\hat{\psi}) = \dfrac{1}{M}\sum_{i=1}^{M}(\hat{\psi}_i - \psi)^2$.

(3) The empirical CP of the 95% confidence or credible intervals, computed as the proportion of intervals that contained the true parameter value.

5.4. Simulation results and discussion

The simulation results are summarized in Table 2. From these results, we observe that both estimation methods perform well across all sample sizes, and their accuracy improves as n increases. The Bayesian estimates are slightly more stable for small samples, showing smaller MSEs and CPs closer to the nominal 95% level. For large samples ($n \geq 200$), both methods yield nearly identical results, confirming their consistency and asymptotic equivalence.

Furthermore, the Bayesian credible intervals tend to be shorter and more accurate than the asymptotic ML intervals. Overall, the findings indicate that while both methods provide reliable inference for the EML model, the Bayesian approach offers more robust performance for small to moderate sample sizes, whereas the ML method remains computationally efficient and accurate for larger samples.

Table 2. Simulation results: average estimates, MSE, and coverage probabilities for (θ, α).

	MLE						Bayes					
	θ			α			θ			α		
						$(\theta, \alpha) = (1, 1.5)$						
n	APE	MSE	CP	APE	MSE	CP	APE	MSE	CP	APE	MSE	CP
30	1.0619	0.05336	0.955	1.6811	0.3398	0.963	1.0506	0.05111	0.95	1.6839	0.35341	0.954
50	1.0507	0.03107	0.958	1.6518	0.20115	0.964	1.0443	0.03003	0.955	1.6525	0.20552	0.943
100	1.0203	0.01495	0.944	1.5593	0.07261	0.952	1.0172	0.01478	0.944	1.5587	0.07307	0.944
150	1.0081	0.00908	0.947	1.5322	0.04524	0.955	1.0061	0.00902	0.943	1.532	0.04543	0.955
200	1.0081	0.00695	0.942	1.5249	0.0349	0.943	1.0066	0.00693	0.94	1.5247	0.03517	0.941
500	1.0059	0.00249	0.963	1.5119	0.01191	0.953	1.0053	0.00248	0.964	1.5118	0.01194	0.949
						$(\theta, \alpha) = (1.5, 2)$						
30	1.5991	0.12628	0.939	2.3646	0.97172	0.969	1.5817	0.12083	0.934	2.3788	1.03127	0.945
50	1.5607	0.06482	0.946	2.1811	0.37956	0.964	1.5503	0.06279	0.944	2.1848	0.38907	0.947
100	1.5272	0.02728	0.953	2.0887	0.14185	0.97	1.5219	0.02678	0.955	2.0893	0.14294	0.955
150	1.5197	0.0185	0.959	2.059	0.09381	0.957	1.5162	0.01828	0.956	2.0599	0.0948	0.949
200	1.5144	0.01329	0.95	2.0403	0.06169	0.954	1.5118	0.01319	0.951	2.0405	0.06212	0.951
500	1.5066	0.00557	0.949	2.0191	0.02388	0.962	1.5055	0.00559	0.947	2.0191	0.024	0.959
						$(\theta, \alpha) = (2, 1.5)$						
30	2.1481	0.23859	0.952	1.7104	0.34504	0.963	2.1233	0.22542	0.953	1.7056	0.34807	0.942
50	2.0653	0.12412	0.948	1.5955	0.16865	0.946	2.0517	0.12086	0.95	1.5925	0.16977	0.934
100	2.0505	0.0562	0.953	1.5592	0.06221	0.958	2.0439	0.0551	0.949	1.5577	0.06223	0.957
150	2.0319	0.04008	0.939	1.54	0.04507	0.939	2.0273	0.03962	0.944	1.5386	0.04493	0.929
200	2.0296	0.02843	0.945	1.5364	0.03102	0.953	2.0265	0.02822	0.941	1.5357	0.03113	0.945
500	2.0079	0.01088	0.945	1.508	0.01138	0.947	2.0067	0.01089	0.945	1.5079	0.01142	0.946
						$(\theta, \alpha) = (2, 2)$						
30	2.1492	0.22615	0.941	2.3445	0.98225	0.971	2.1244	0.21373	0.937	2.3539	1.03612	0.951
50	2.0885	0.12208	0.945	2.1856	0.38126	0.966	2.0746	0.11868	0.934	2.1886	0.39109	0.941
100	2.037	0.05068	0.954	2.0837	0.14484	0.95	2.0296	0.04998	0.952	2.0836	0.14623	0.939
150	2.0222	0.03343	0.951	2.0513	0.08402	0.945	2.0177	0.03322	0.945	2.0517	0.08491	0.939
200	2.0236	0.02522	0.953	2.0471	0.06189	0.953	2.02	0.02485	0.952	2.0472	0.06192	0.953
500	2.0044	0.00999	0.95	2.0128	0.02393	0.944	2.003	0.00993	0.95	2.0125	0.02387	0.944

6. Applications

In this section, we analyze the proposed EML distribution and compare its performance with several closely related lifetime models, including the ML [4], SML [19], PML [13], MOML [8], and NLE [11] distributions, using four medical datasets drawn from different applied contexts. The CDFs of these distributions are provided in Appendix C.

Data 1: The first dataset consists of the estimated time from the initiation of growth hormone therapy to the point at which children reached the targeted developmental age. The data were obtained from the Hormonal Program of the Health Secretariat of Minas Gerais [1]. The data values are given in Appendix D.

Data 2: The second dataset, introduced by Bantan et al. [3], comprises 106 observations representing mortality rates during the COVID-19 pandemic in Mexico, recorded between March 4 and July 20, 2020. For analytical convenience, all observations were rescaled by dividing them by five. Such linear rescaling does not affect the inferential conclusions for the model parameters. The resulting data are given in Appendix D.

Data 3: The third dataset consists of 20 patient lifetimes under analgesic therapy. The data were originally reported by Gross and Clark [9] and later revisited by Shah et al. [18]. The data values are given in Appendix D.

Data 4: The fourth dataset contains daily COVID-19 mortality rate from the Netherlands between March 31 and April 30, 2020 [2]. The data values are given in Appendix D.

Figures 4–7 provide nonparametric diagnostic plots (boxplot, total time on test (TTT) plot, violin plot, and Q–Q plot) for all datasets. These graphical tools allow preliminary assessment of distributional shape and tail behavior:

- **Data 1:** The data are moderately dispersed and right-skewed, with several large values (above 10) indicating a heavy right tail.
- **Data 2:** This dataset has the smallest IQR, showing a tightly concentrated distribution with right skewness and a few high-end observations. Deviations in the upper tail of the Q–Q plot confirm heavy-tail behavior.
- **Data 3:** The data exhibit pronounced right skewness with a high outlier.
- **Data 4:** This dataset shows the greatest dispersion, strong right skewness, and one outlier.

Moreover, the TTT plot for all data sets suggests an increasing failure rate (IFR).

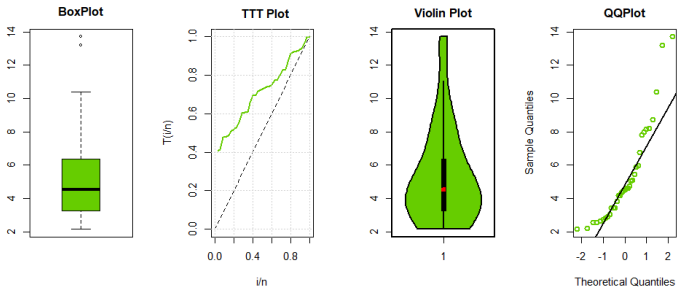

Figure 4. Graphical nonparametric representations of Dataset 1.

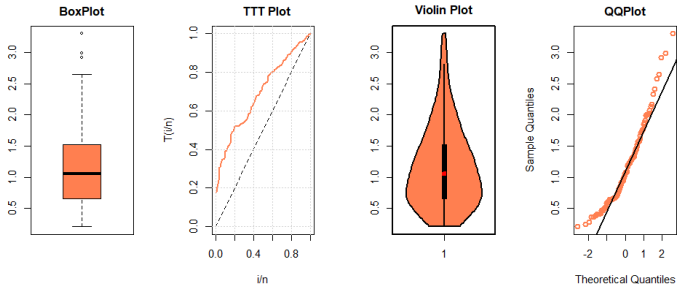

Figure 5. Graphical nonparametric representations of Dataset 2.

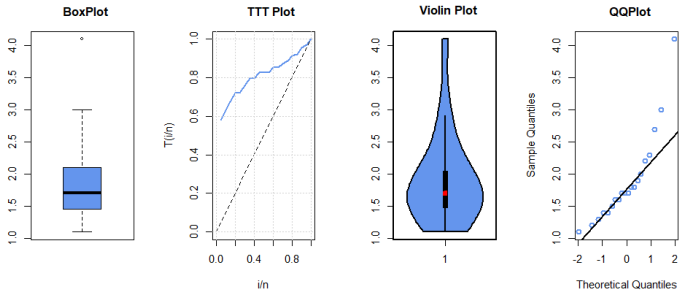

Figure 6. Graphical nonparametric representations of Dataset 3.

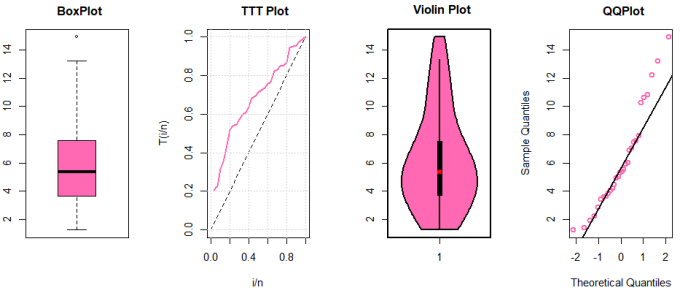

Figure 7. Graphical nonparametric representations of Dataset 4.

Our analysis has three main objectives:

(1) To demonstrate the practical applicability of the EML model using real medical datasets.
(2) To assess whether extending the ML distribution improves fitting performance.
(3) To compare the two generalizations of the ML, PML, and EML based on likelihood and distance-based criteria.

To accomplish this, we compute MLEs, evaluate the log-likelihood at the MLEs, and calculate several model selection criteria: AIC, BIC, CAIC, and HQIC. Additionally, we employ nonparametric goodness-of-fit measures: the Anderson–Darling (A^*), Cramér–von Mises (W^*), and Kolmogorov–Smirnov (K–S) statistics along with their P-values. A model is considered superior when it yields smaller values of the information criteria and test statistics, and larger P-values.

We also conduct likelihood ratio tests (LRTs) comparing the ML and EML models to quantify the improvement gained through model generalization.

6.1. Concluding remarks on data analysis

Parametric results. Table 3 presents the MLEs, standard errors, negative log-likelihood values, and information criteria for all competing models and datasets. Across all four applications, the EML model consistently achieves the smallest AIC, BIC, CAIC, and HQIC values, confirming its superior parametric performance.

Nonparametric results. Table 4 reports the W^*, A^*, and K–S statistics and corresponding P-values. For every dataset, the EML distribution attains the smallest test-statistic values and the largest P-values, further confirming its excellent goodness-of-fit relative to the alternative models.

Table 3. The MLE(SE), $-\mathcal{L}$, AIC, BIC, CAIC, and HQIC for all models using the four datasets.

Model	$\hat{\theta}$(SE)	$\hat{\alpha}$(SE)	$-\mathcal{L}$	AIC	BIC	CAIC	HQIC
			Data 1				
ML	$\hat{\theta}$ = 0.2189(0.0285)	-	86.5219	175.0440	176.5993	175.1652	175.5809
SML	$\hat{\theta}$ = 0.1487(0.0167)	-	84.4437	170.8874	172.4428	171.0087	171.4243
PML	$\hat{\theta}$ = 0.0834(0.0271)	$\hat{\alpha}$ = 1.5575(0.1788)	80.8252	165.6503	168.7610	166.0253	166.7242
MOML	$\hat{\theta}$ = 0.5243(0.1140)	$\hat{\alpha}$ = 9.9372(6.9927)	82.5778	169.1555	172.2662	169.5305	170.2293
NLE	$\hat{\theta}$ = 0.2036(0.0167)	$\hat{\alpha}$ = 1.7614(0.2479)	80.1305	164.2610	167.3716	164.6360	165.3348
EML	$\hat{\theta}$ = 0.4481(0.0799)	$\hat{\alpha}$ = 4.4901(1.7426)	78.8368	161.6737	164.7844	162.0487	162.7475
			Data 2				
ML	$\hat{\theta}$ = 0.9359(0.0745)	-	110.4736	222.9472	225.6106	222.9857	224.0267
SML	$\hat{\theta}$ = 0.6168(0.0417)	-	104.3267	210.6534	213.3168	210.6918	211.7329
PML	$\hat{\theta}$ = 0.7828(0.0700)	$\hat{\alpha}$ = 1.6130(0.1168)	93.67205	191.3441	196.6710	191.4606	193.5031
MOML	$\hat{\theta}$ = 0.9686(0.0734)	$\hat{\alpha}$ = 1.4959(0.0943)	94.2649	192.5299	197.8567	192.6464	194.6889
NLE	$\hat{\theta}$ = 0.8385(0.0436)	$\hat{\alpha}$ = 1.7164(0.1391)	92.9019	189.8038	195.1307	189.9203	191.9628
EML	$\hat{\theta}$ = 1.7166(0.1735)	$\hat{\alpha}$ = 3.2614(0.6029)	91.3096	186.6192	191.9461	186.7357	188.7782
			Data 3				
ML	$\hat{\theta}$ = 0.5774(0.1017)	-	29.0072	60.0144	61.0102	60.2366	60.2088
SML	$\hat{\theta}$ = 0.3954(0.0591)	-	27.0303	56.0605	57.0563	56.2828	56.2549
PML	$\hat{\theta}$ = 0.2274(0.0709)	$\hat{\alpha}$ = 2.3398(0.3374)	19.2199	42.4399	44.4314	43.1458	42.8287
MOML	$\hat{\theta}$ = 0.3899(0.0865)	$\hat{\alpha}$ = 2.0343(0.2622)	19.7845	43.5690	45.5605	44.2749	43.9578
NLE	$\hat{\theta}$ = 0.5137(0.0322)	$\hat{\alpha}$ = 3.1547(0.5996)	17.2014	38.4028	40.3943	39.1086	38.7916
EML	$\hat{\theta}$ = 2.1765(0.4487)	$\hat{\alpha}$ = 32.1017(23.4038)	16.1809	36.3619	38.3533	37.0678	36.7506
			Data 4				
ML	$\hat{\theta}$ = 0.19009(0.0267)	-	79.5508	161.1017	162.5029	161.2445	161.5499
SML	$\hat{\theta}$ = 0.1279(0.0155)	-	78.1325	158.2649	159.6661	158.4078	158.7132
PML	$\hat{\theta}$ = 0.0906(0.0342)	$\hat{\alpha}$ = 1.3914(0.1803)	76.8322	157.6644	160.4668	158.1089	158.5609
MOML	$\hat{\theta}$ = 0.3835(0.0985)	$\hat{\alpha}$ = 6.2689(4.8853)	77.4315	158.8630	161.6654	159.3075	159.7595
NLE	$\hat{\theta}$ = 0.1768(0.0185)	$\hat{\alpha}$ = 1.4686(0.2274)	76.9250	157.8500	160.6524	158.2945	158.7465
EML	$\hat{\theta}$ = 0.2883(0.0564)	$\hat{\alpha}$ = 2.2302(0.7518)	76.8178	157.6356	160.4380	158.0800	158.5321

Table 4. The values of non-parametric statistics for the four datasets.

Model	W*	A*	K-S	P-value	W*	A*	KS	P-value
	Data 1				Data 2			
ML	0.0798	0.4760	0.0918	0.2307	0.0619	0.3617	0.1762	0.0028
SML	0.1131	0.7253	0.1979	0.1291	0.0751	0.4584	0.1499	0.0171
PML	0.1179	0.7535	0.1235	0.6596	0.0992	0.6259	0.0718	0.6460
MOML	0.1552	0.9609	0.1304	0.5909	0.1105	0.7007	0.0689	0.6957
NLE	0.0891	0.5893	0.0937	0.9182	0.0849	0.4954	0.0749	0.5907
EML	0.0618	0.4251	0.0916	0.9306	0.0576	0.3184	0.0676	0.7185
	Data 3				Data 4			
ML	0.1026	0.6078	0.3571	0.0122	0.0235	0.1767	0.1671	0.3340
SML	0.1143	0.6771	0.3419	0.0186	0.0291	0.2015	0.1359	0.5898
PML	0.1471	0.8679	0.1779	0.5513	0.0281	0.1967	0.0815	0.9789
MOML	0.1622	0.9509	0.1683	0.6230	0.0445	0.2898	0.0845	0.9707
NLE	0.0773	0.4593	0.1273	0.9024	0.0217	0.1724	0.0818	0.9781
EML	0.0524	0.3071	0.1335	0.8680	0.0214	0.1749	0.0761	0.9897

Likelihood-based confidence intervals. Approximate 95% confidence intervals using 14.7% MLI for the EML parameters are provided in Table 5. These intervals quantify parameter uncertainty and are consistent with the MLE-based conclusions.

Table 5. The 14.7% likelihood intervals for the EML parameters, using the four datasets.

Par	Data 1	Data 2	Data 3	Data 4
θ	(0.3848, 0.5215)	(1.5474, 1.9033)	(1.9328, 2.4715)	(0.2337, 0.3535)
α	(3.1665, 6.1407)	(2.6828, 3.9193)	(20.2305, 48.5471)	(1.5269, 3.1186)

Bootstrap confidence intervals. To further assess parameter uncertainty, we computed four types of bootstrap confidence intervals for θ and α (normal, basic, percentile, and BCa), as summarized in Table 6. Figure 8 displays the empirical bootstrap sampling distributions of the parameter estimates.

Table 6. The bootstrap 95% confidence intervals for θ and α using all datasets.

	Data 1		Data 2	
Method	θ	α	θ	α
Normal	(0.2471, 0.6066)	(-0.6339, 8.0885)	(1.3779, 2.0020)	(2.0261, 4.2474)
Basic	(0.2179, 0.5725)	(-2.0885, 6.3296)	(1.3491, 1.9726)	(1.8359, 4.0518)
Percentile	(0.3236, 0.6782)	(2.6512, 11.0693)	(1.4598, 2.0834)	(2.4700, 4.6860)
BCa	(0.2961, 0.6283)	(2.3596, 8.7507)	(1.4227, 2.0315)	(2.3524, 4.3930)
	Data 3		Data 4	
Normal	(0.7697, 3.2071)	(-645.94, 608.38)	(0.1600, 0.3832)	(-0.5089, 4.1706)
Basic	(0.5423, 2.9459)	(-298.25, 54.343)	(0.1358, 0.3605)	(-1.1055, 3.0412)
Percentile	(1.4148, 3.8184)	(10.301, 362.89)	(0.2162, 0.4409)	(1.4212, 5.5679)
BCa	(1.1983, 3.2912)	(7.6839, 174.73)	(0.1988, 0.3954)	(1.2709, 4.2212)

As noted earlier, the lower bounds of the normal and basic confidence intervals for α are negative, which is not permissible. Therefore, we prefer the remaining two confidence intervals.

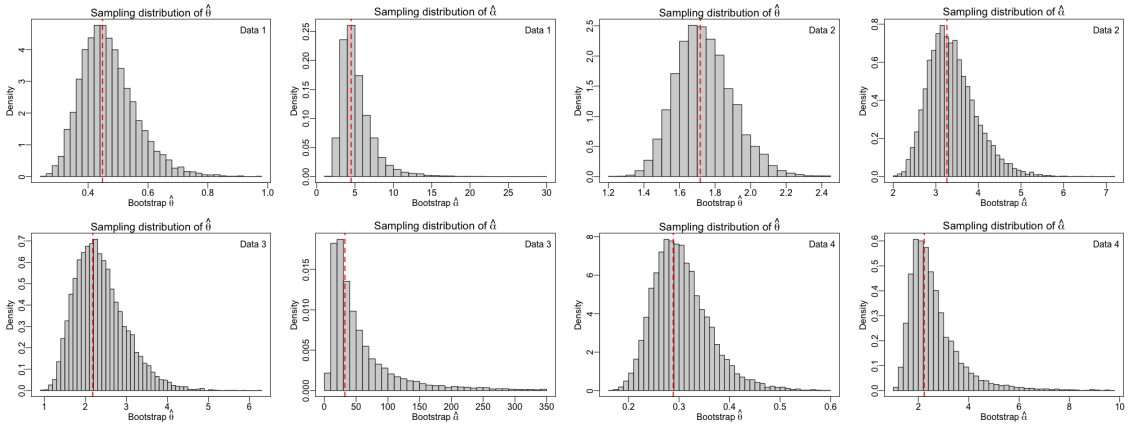

Figure 8. Bootstrap sampling distributions for $\hat{\theta}$ and $\hat{\alpha}$, using the four datasets.

Hypothesis testing (LRT). We conducted likelihood ratio tests to evaluate whether the EML generalization provides a statistically significant improvement over the ML model. Specifically, we tested

$$H_0 : \alpha = 1 \quad \text{(ML model)} \quad \text{vs.} \quad H_1 : \alpha \neq 1 \quad \text{(EML model)}.$$

The LRT statistic $\Lambda = -2(\mathcal{L}_0 - \mathcal{L}_1)$ is asymptotically χ^2_1 under H_0. Table 7 reports the LRT statistics and P-values for all four datasets. In all cases, the null hypothesis is rejected, indicating that the EML model provides a significantly better fit.

Table 7. Likelihood ratio test statistics and corresponding P-values.

Statistic	Data 1	Data 2	Data 3	Data 4
Λ	15.3902	38.3280	25.6526	5.4660
P-value	8.744×10^{-5}	5.9798×10^{-10}	4.0874×10^{-7}	0.01939

Relative log-likelihood and uniqueness of MLE. Figure 9 displays the relative log-likelihood functions and the likelihood intervals for each model and dataset. Each plot shows a single global maximum, supporting the uniqueness and stability of the MLEs reported above.

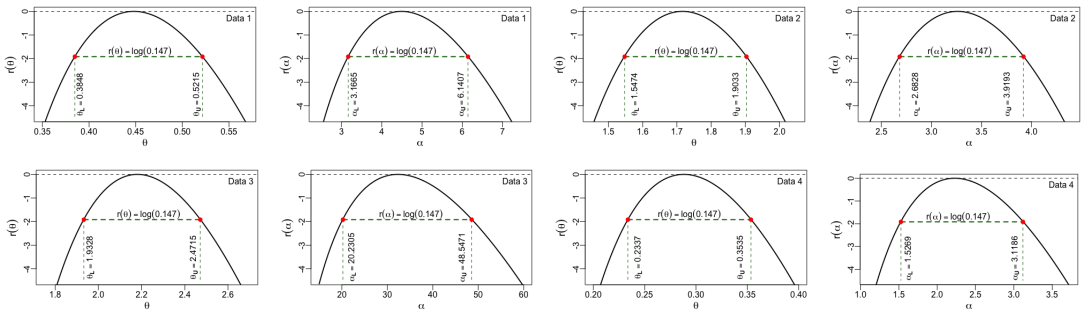

Figure 9. Relative log-likelihood functions along with the likelihood intervals for the four datasets.

Empirical and fitted CDFs/PDFs. Figures 10 and 11 show the empirical vs. fitted CDFs and PDFs for the four datasets under the competing models, illustrating visually the improved fit of the EML

distribution.

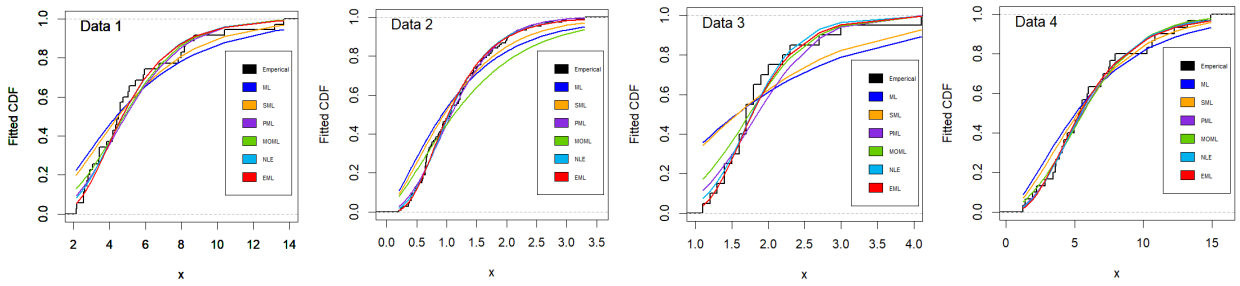

Figure 10. Empirical and fitted CDFs of the four datasets using the competing models.

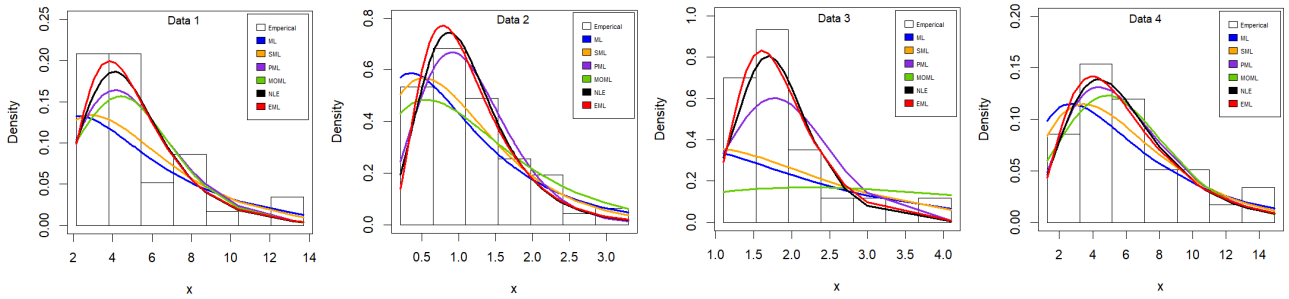

Figure 11. Empirical and estimated PDFs of the four datasets using the competing models.

6.2. Bayesian inferences

We assumed the absence of prior information about the model parameters; therefore, the hyperparameters of the gamma prior distributions were set to small values ($a_1 = a_2 = b_1 = b_2 = 0.001$), representing vague or noninformative priors. Based on this assumption, we implemented the MCMC algorithm described earlier to generate 10,000 samples of (θ, α) from the joint posterior distribution. To ensure convergence and reduce the influence of the initial values, the first 50% of the samples were discarded as burn-in, and the remaining 50% were retained for posterior inference.

As a diagnostic assessment of the simulated draws, Figure 12 presents the contour plot of the joint posterior distribution of (θ, α), overlaid with the simulated draws, together with the marginal posterior densities of θ and α. Furthermore, Figure 13 displays the trace plots of the marginal draws along with their corresponding autocorrelation functions. The figures clearly show that the simulated samples align well with the high-density regions of the posterior distribution, confirming that the MCMC algorithm adequately explored the target distribution. Additionally, the autocorrelation function (ACF) decays to nearly zero by lag 12, indicating that the Markov chain achieved good mixing and that successive draws became approximately independent.

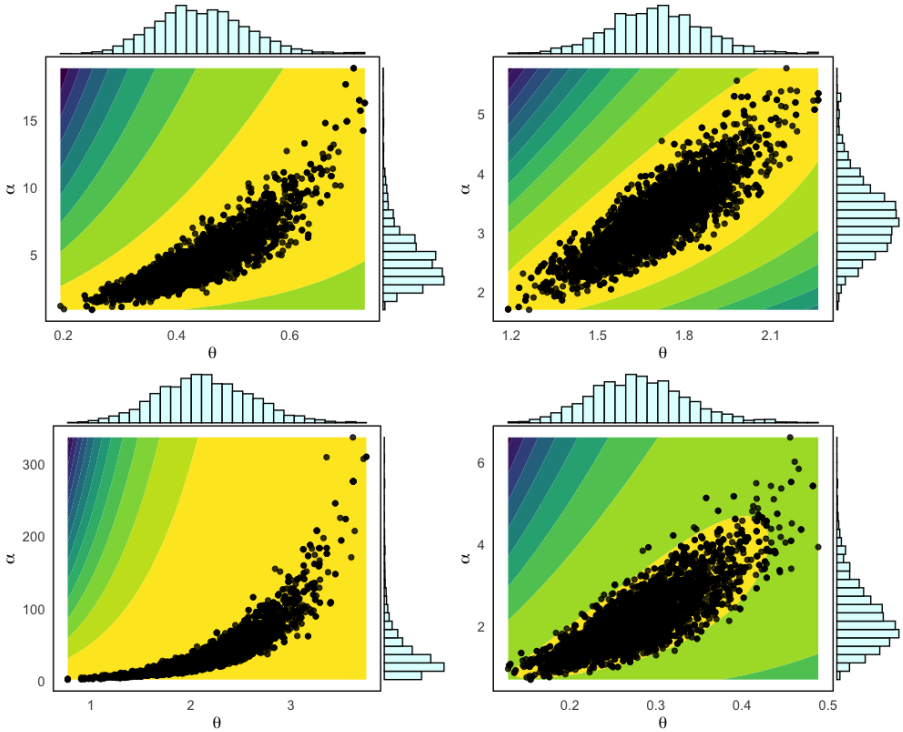

Figure 12. Contour plots for the posterior distributions along with the simulated draws from from the MCMC method and the approximated marginal posterior distributions of the model parameters.

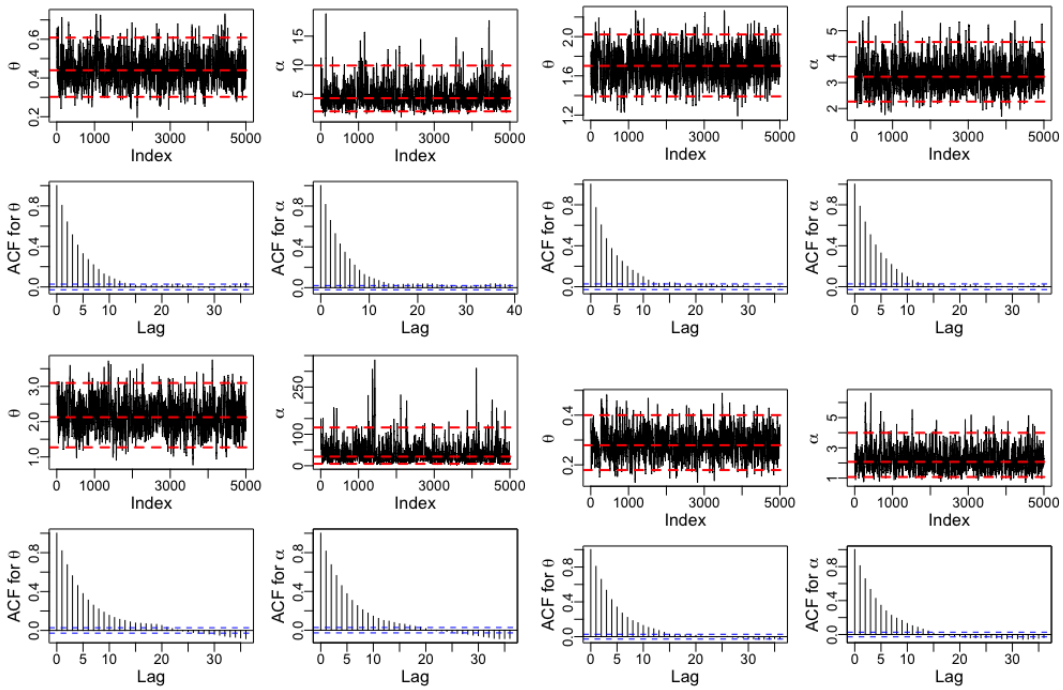

Figure 13. Trace plots and corresponding autocorrelation plots for θ and α based on Data 1 and 2 (left to right, first row) and Data 3 and 4 (left to right, second row).

Table 8 presents the Bayesian point estimates, the corresponding minimum Bayes risks (MBRs), and the 95% credible intervals for each parameter across all datasets. As expected, the Bayesian estimates closely align with the MLEs, demonstrating consistency between the two approaches.

Table 8. The Bayesian results.

	Data 1			Data 2		
Par	BE	MBR	95% CI	BE	MBR	95% CI
θ	0.4444	0.0064	(0.3025, 0.6085)	1.7031	0.0263	(1.3906, 2.0228)
α	4.7256	4.2775	(2.0545, 9.9444)	3.2603	0.3464	(2.2675, 4.5649)
	Data 3			Data 4		
θ	2.1409	0.2165	(1.2715, 3.096)	0.281	0.0031	(0.179, 0.4001)
α	37.939	1059.09	(6.1286, 121.5953)	2.1978	0.5757	(1.0709, 3.9937)

A comparison between the frequentist results presented in Table 4 and the Bayesian estimates reported in Table 8 reveals a strong agreement between the two approaches. Specifically, the Bayesian estimates are nearly identical to the corresponding MLEs. This close correspondence is anticipated, as the hyperparameters of the prior distributions were deliberately set to very small values, thereby representing vague or noninformative priors that exert minimal influence on the posterior inference.

This consistency between the Bayesian and frequentist approaches demonstrates the robustness of the proposed estimation framework and validates the numerical stability of the developed methods. Moreover, it highlights that the likelihood function plays a dominant role in shaping the inference when prior information is weak or unavailable. Consequently, the proposed model can be confidently applied in practical situations where prior knowledge about the parameters is limited, ensuring reliable and data-driven parameter estimation.

7. Conclusions

In this work, we proposed a versatile two-parameter extension of the modified Lindley distribution, termed the exponentiated modified Lindley (EML) distribution. Several theoretical arguments were presented to justify the development of this new model. A comprehensive investigation of its fundamental properties was carried out, including the behavior of its density and hazard functions, its moments and incomplete moments, the moment generating function, and associated measures of skewness and kurtosis.

Parameter estimation was explored through both maximum likelihood and Bayesian frameworks, supported by an extensive simulation study designed to evaluate and compare estimator performance. In addition, approximate likelihood-based confidence intervals for the EML parameters were constructed, and a practical algorithm was provided for generating various bootstrap confidence intervals. A likelihood ratio test was also employed to assess the adequacy of the EML distribution relative to its baseline counterpart.

The utility of the EML model was illustrated through four real medical datasets. Across all empirical analyses, the proposed distribution delivered superior goodness-of-fit results when compared with several established competing models. Overall, the findings confirm that the EML distribution is a flexible and powerful tool for modeling real-world data.

Author contributions

Ammar M. Sarhan and M. E. Sobh: Conceptualization, writing original draft, writing–review, resources, formal analysis, software, investigation, methodology, supervision; Asamh Saleh M. Al Luhayb and Reid Alotaibi: Validation, data curation, investigation; All authors have read and agreed to the published version of the manuscript.

Use of Generative-AI tools declaration

The authors declare that they have not used Artificial Intelligence (AI) tools in the creation of this article.

Acknowledgments

The researchers would like to thank the Deanship of Graduate Studies and Scientific Research at Qassim University for the financial support (QU-APC-2026).

Conflicts of interest

Prof. Ammar M. Sarhan is the Guest Editor of special issue "Lifetime Distributions and Statistical Methods with Applications to Real Scientific Problems" for AIMS Mathematics. Prof. Ammar M. Sarhan was not involved in the editorial review or the decision to publish this article.

All authors declare no conflicts of interest in this paper.

Appendix

A. MLI and likelihood ratio χ^2 approximation

Let $\mathcal{L}(\theta)$ denote the log-likelihood function and $\hat{\theta}$ its MLE. The 100p% MLI for θ, $0 < p < 1$, is defined by the criterion

$$r(\theta) = \mathcal{L}(\hat{\theta}) - \mathcal{L}(\theta) \geq \log p.$$

For large samples, the likelihood ratio statistic

$$\Lambda(\theta) = -2[\mathcal{L}(\theta) - \mathcal{L}(\hat{\theta})]$$

asymptotically follows a χ^2_1 distribution under standard regularity conditions. Rewriting the MLI criterion in terms of $\Lambda(\theta)$ gives

$$\Lambda(\theta) \leq -2 \log p.$$

Comparing this with the χ^2 quantiles, the threshold p is related to the nominal $(1 - \delta)100\%$ CI by

$$p = \exp\Big(-\frac{1}{2}\chi^2_{1,1-\delta}\Big),$$

which ensures that the MLI has approximately the desired coverage.

B. Bootstrap approaches

(i) Normal approximation (standard bootstrap) interval

This interval assumes that the sampling distribution of $\hat{\theta}$ is approximately normal. The $(1-\delta)100\%$ confidence interval is given by

$$CI_{\text{Normal}} = \left(\hat{\theta} - z_{\delta/2}\widehat{SE}_{boot},\ \hat{\theta} + z_{\delta/2}\widehat{SE}_{boot}\right), \tag{B1}$$

where $\widehat{SE}_{boot}$ is the bootstrap estimate of the standard error,

$$\widehat{SE}_{boot} = \sqrt{\frac{1}{B-1}\sum_{b=1}^{B}\left(\hat{\theta}^{*(b)} - \bar{\hat{\theta}}^{*}\right)^2},$$

and $z_{\delta/2}$ is the upper $\delta/2$ quantile of the standard normal distribution. This approach is simple but may perform poorly when the sampling distribution of $\hat{\theta}$ is skewed or non-normal.

(ii) Basic bootstrap interval

The basic (or pivotal) bootstrap interval is based on the symmetry of the bootstrap distribution around the original estimate $\hat{\theta}$. It is defined as

$$CI_{\text{Basic}} = \left(2\hat{\theta} - \hat{\theta}^{*}_{(1-\delta/2)},\ 2\hat{\theta} - \hat{\theta}^{*}_{(\delta/2)}\right), \tag{B2}$$

where $\hat{\theta}^{*}_{(p)}$ denotes the pth quantile of the bootstrap distribution. This interval corrects for potential bias and is invariant under monotone transformations of the parameter.

(iii) Percentile bootstrap interval

The percentile interval directly uses the empirical quantiles of the bootstrap distribution of $\hat{\theta}^{*}$:

$$CI_{\text{Percentile}} = \left(\hat{\theta}^{*}_{(\delta/2)},\ \hat{\theta}^{*}_{(1-\delta/2)}\right). \tag{B3}$$

This method is intuitive and easy to compute, as it does not require estimation of the standard error. However, it assumes that the bootstrap distribution is centered at the true parameter value, which may not always hold.

(iv) Bias-corrected and accelerated (BCa) bootstrap interval

The BCa interval, proposed by Efron [7], improves upon the percentile method by accounting for both bias and skewness in the bootstrap distribution. It adjusts the percentiles using two parameters: the bias-correction factor z_0 and the acceleration constant a. The $(1-\delta)100\%$ BCa confidence interval is given by

$$CI_{\text{BCa}} = \left(\hat{\theta}^{*}_{\left(\Phi\left[z_0 + \frac{z_0 + z_{\delta/2}}{1 - a(z_0 + z_{\delta/2})}\right]\right)},\ \hat{\theta}^{*}_{\left(\Phi\left[z_0 + \frac{z_0 + z_{1-\delta/2}}{1 - a(z_0 + z_{1-\delta/2})}\right]\right)}\right), \tag{B4}$$

where $\Phi(\cdot)$ denotes the cumulative distribution function of the standard normal distribution. The BCa interval generally provides superior coverage accuracy, particularly in small-sample or skewed distributions.

C. CDF used in Section 6

The CDF of distributions, used in Section 6, are listed below:

- For ML [4], this is already given in Eq (1.1).
- For SML [19]:

$$F(x;\theta) = \cos\left[\frac{\pi}{2}\left(1+\frac{\theta x}{1+\theta}e^{-\theta x}\right)e^{-\theta x}\right],\ x>0,\ \theta>0. \tag{C1}$$

- For PML [13]:

$$F(x;\theta,\alpha) = 1-\left(1+\frac{\theta x^{\alpha}}{1+\theta}e^{-\theta x^{\alpha}}\right)e^{-\theta x^{\alpha}}, \qquad x>0,\ \theta>0,\ \alpha>0. \tag{C2}$$

- For MOML [8]:

$$F(x;\theta,\alpha) = 1-\frac{\alpha\left(\frac{1+\frac{\theta x}{1+\theta}e^{-\theta x}}{1+\theta}\right)e^{-\theta x}}{1-(1-\alpha)\left(\frac{1+\frac{\theta x}{1+\theta}e^{-\theta x}}{1+\theta}\right)e^{-\theta x}}, \qquad x>0,\ \theta,\alpha>0. \tag{C3}$$

- For NLE [11]:

$$F(x;\theta,\alpha) = \frac{\left[1-e^{-\theta x}\left(1+\frac{\theta x e^{-\theta x}}{\theta+1}\right)\right]^{\alpha}}{\left[1-e^{-\theta x}\left(1+\frac{\theta x e^{-\theta x}}{\theta+1}\right)\right]^{\alpha}+\left[e^{-\theta x}\left(1+\frac{\theta x e^{-\theta x}}{\theta+1}\right)\right]^{\alpha}},\ x>0,\ \theta,\alpha>0. \tag{C4}$$

D. Data used in Section 6

Data 1:
2.15, 2.20, 2.55, 2.56, 2.63, 2.74, 2.81, 2.90, 3.05, 3.41, 3.43, 3.43, 3.84, 4.16, 4.18, 4.36, 4.42, 4.51, 4.60, 4.61, 4.75, 5.03, 5.10, 5.44, 5.90, 5.96, 6.77, 7.82, 8.00, 8.16, 8.21, 8.72, 10.40, 13.20, 13.70.

Data 2:
1.7652, 1.2210, 1.8782, 2.9942, 2.0766, 1.4534, 2.6440, 3.2996, 2.3330, 1.2030, 2.1710, 1.2244, 1.3312, 0.6880, 1.1708, 2.1370, 2.0070, 1.0484, 0.8668, 1.0286, 1.5260, 2.9208, 1.5806, 1.2740, 0.7074, 1.2654, 0.9460, 0.6430, 1.8568, 2.5756, 1.7626, 2.0086, 1.4520, 1.1970, 1.2824, 0.6790, 0.8848, 1.9870, 1.5680, 1.9100, 0.6998, 0.7502, 1.3936, 0.6572, 2.0316, 1.6216, 1.3394, 1.4302, 1.3120, 0.4154, 0.7556, 0.5976, 0.6672, 1.3628, 1.5708, 1.6650, 1.7120, 0.6456, 1.4972, 1.3250, 1.2280, 0.9818, 0.9322, 1.0784, 2.4084, 1.7392, 0.3630, 0.6654, 1.0812, 1.2364, 0.2082, 0.3600, 0.9898, 0.8178, 0.6718, 0.4140, 0.6596, 1.0634, 1.0884, 0.9114, 0.8584, 0.5000, 1.3070, 0.9296, 0.9394, 1.0918, 0.8240, 0.7884, 0.6438, 0.2804, 0.4876, 0.6514, 0.7264, 0.6466, 0.6054, 0.4704, 0.2410, 0.6436, 0.5852, 0.5202, 0.4130, 0.6058, 0.4116, 0.4652, 0.5052, 0.3846.

Data 3:
1.4, 1.1, 1.7, 1.3, 1.8, 1.9, 2.2, 1.6, 2.7, 1.7, 1.8, 4.1, 1.2, 1.5, 3.0, 1.4, 2.3, 1.7, 2.0, 1.6.

Data 4:
14.918, 10.656, 12.274, 10.289, 10.832, 7.968, 7.584, 5.555, 6.027, 7.099, 5.928, 13.211, 4.097, 3.611, 4.960, 7.498, 6.940, 5.307, 5.048, 2.857, 2.254, 5.431, 4.462, 3.883, 3.461, 3.647, 1.974, 1.273, 1.416, 4.235.

References

1. M. Alizadeh, S. F. Bagheri, E. B. Samani, S. Ghobadi, S. Nadarajah, Exponentiated power Lindley power series class of distributions: theory and applications, *Commun. Stat.–Simul. Comput.*, **47** (2018), 2499–2531. https://doi.org/10.1080/03610918.2017.1350270
2. H. M. Almongy, E. M. Almetwally, H. M. Aljohani, A. S. Alghamdi, E. H. Hafez, A new extended Rayleigh distribution with applications of COVID-19 data, *Results Phys.*, **23** (2021), 104012. https://doi.org/10.1016/j.rinp.2021.104012
3. R. A. Bantan, Z. Ahmad, F. Khan, M. Elgarhy, Z. Almaspoor, G. G. Hamedani, et al., Predictive modeling of the COVID-19 data using a new version of the flexible Weibull model and machine learning techniques, *Math. Biosci. Eng.*, **20** (2023), 2847–2873. https://doi.org/10.3934/mbe.2023134
4. C. Chesneau, L. Tomy, J. Gillariose, A new modified Lindley distribution with properties and applications, *J. Stat. Manag. Syst.*, **24** (2021), 1383–1403. https://doi.org/10.1080/09720510.2020.1824727
5. A. C. Davison, D. V. Hinkley, *Bootstrap methods and their application*, Cambridge University Press, 1997.
6. B. Efron, Bootstrap methods: another look at the jackknife, *Ann. Statist.*, **7** (1979), 1–26. https://doi.org/10.1214/aos/1176344552
7. B. Efron, Better bootstrap confidence intervals, *J. Am. Stat. Assoc.*, **82** (1987), 171–185. https://doi.org/10.2307/2289144
8. J. Gillariose, L. Tomy, F. Jamal, C. Chesneau, The Marshall–Olkin modified Lindley distribution: properties and applications, *J. Reliab. Stat. Stud.*, **13** (2020), 177–198. https://doi.org/10.13052/jrss0974-8024.1319
9. A. J. Gross, V. Clark, *Survival distributions: reliability applications in the biomedical sciences*, John Wiley & Sons, 1975.
10. R. D. Gupta, D. Kundu, Theory & methods: generalized exponential distributions, *Australian & New Zealand J. Stat.*, **41** (1999), 173–188. https://doi.org/10.1111/1467-842X.00072
11. M. Hashempour, M. Alizadeh, H. M. Yousof, A new Lindley extension: estimation, risk assessment and analysis under bimodal right skewed precipitation data, *Ann. Data Sci.*, **11** (2024), 1919–1958. https://doi.org/10.1007/s40745-023-00485-1
12. J. G. Kalbfleisch, *Probability and statistical inference*, Vol. 2, New York: Springer, 1985.

13. O. Kharazmi, D. Kumar, S. Dey, Power modified Lindley distribution: properties, classical and Bayesian estimation, and regression model with applications, *Aust. J. Stat.*, **52** (2023), 71–95. https://doi.org/10.17713/ajs.v52i3.1386

14. G. S. Mudholkar, D. K. Srivastava, Exponentiated Weibull family for analyzing bathtub failure-rate data, *IEEE Trans. Reliab.*, **42** (1993), 299–302. https://doi.org/10.1109/24.229504

15. A. M. Sarhan, J. Apaloo, Exponentiated modified Weibull extension distribution, *Reliab. Eng. Syst. Safe.*, **112** (2013), 137–144. https://doi.org/10.1016/j.ress.2012.10.013

16. A. M. Sarhan, A. Abd EL-Baset, I. A. Alasbahi, Exponentiated generalized linear exponential distribution, *Appl. Math. Model.*, **37** (2013), 2838–2849. https://doi.org/10.1016/j.apm.2012.06.019

17. A. M. Sarhan, D. Kundu, Generalized linear failure rate distribution, *Commun. Stat.- Theory Methods*, **38** (2009), 642–660. https://doi.org/10.1080/03610920802272414

18. Z. Shah, A. Ali, M. Hamraz, D. M. Khan, Z. Khan, M. El-Morshedy, et al., A new member of T–X family with applications in different sectors, *J. Math.*, **2022** (2022), 1453451. https://doi.org/10.1155/2022/1453451

19. L. Tomy, V. G, C. Chesneau, The sine modified Lindley distribution, *Math. Comput. Appl.*, **26** (2021), 81. https://doi.org/10.3390/mca26040081

20. S. Zacks, Estimating the shift to wear-out of systems having exponential-Weibull life distributions, *Oper. Res.*, **32** (1984), 741–749. https://doi.org/10.1287/opre.32.3.741

AIMS Press